SPANDIDOS PUBLICATIONS

ONCOLOGY REPORTS 41: 501-511, 2019

In vitro neutralization of autocrine IL-10 affects Op18/stathmin signaling in non-small cell lung cancer cells

YAN ZHAO[1], SANGYAN CHEN[1], FANG SHEN[2], DAN LONG[1], TING YU[1], MENGRU WU[1] and XUECHI LIN[1,2]

[1]Department of Medical Laboratory, Changsha Medical University; [2]Department of Clinical Laboratory, The First Affiliated Hospital of Hunan Normal University, Changsha, Hunan 410219, P.R. China

Received January 5, 2018; Accepted September 17, 2018

DOI: 10.3892/or.2018.6795

Abstract. Our previous studies have identified that silencing oncoprotein 18 (Op18)/stathmin via RNA interference (RNAi) inhibited autocrine interleukin-10 (IL-10) and enhanced the sensitivity to Taxol in NCI-H1299 non-small cell lung cancer cells. In this study, whether autocrine IL-10 regulates Op18/stathmin signaling in NCI-H1299 cells was examined by neutralizing IL-10 using a targeted antibody. *In vitro* neutralization of IL-10 by anti-IL-10 antibody impaired the capacities of the NCI-H1299 cells to proliferate, form colonies and migrate. Furthermore, the expression levels of caspase-3 and -8, and sensitivity to Taxol were increased. Neutralizing IL-10 down-regulated Op18/stathmin expression and its phosphorylation at Ser25 and Ser63 sites, and suppressed the activities of upstream kinases, extracellular signal-regulated kinase (ERK) and cyclin-dependent kinase 1 (CDK1). In addition, neutralizing IL-10 also reduced the expression levels of the transcription factor nuclear factor-κB (NF-κB) and phosphorylation of its active subunit, p65 (Ser536). Furthermore, blocking NF-κB signaling with PDTC also decreased the activities of ERK and CDC2 kinases, and decreases levels of autocrine released IL-10 and its protein expression. Additionally, knocking down Op18/stathmin by RNAi reduced the expression levels of NF-κB and IL-10. Further animal experiments revealed that the number of neutrophils, lymphocytes and monocytes were all decreased in the blood of tumor-bearing mice with NCI-H1299 cell xenografts. Thus, the data suggested that autocrine IL-10 regulates Op18/stathmin signaling via an IL-10-NF-κB-ERK/CDC2 axis, which regulates the malignant behaviors of NCI-H1299 cells. A feedback regulation also exists between Op18/stathmin and autocrine IL-10 signaling pathways in non-small cell lung cancer cells.

Correspondence to: Professor Xuechi Lin, Department of Medical Laboratory, Changsha Medical University, 9th Kilometer's Stop at Leifeng Road, Wangcheng, Changsha, Hunan 410219, P.R. China
E-mail: xuechilin71@126.com

Key words: autocrine IL-10, neutralization, Op18/stathmin, NF-κB, signaling regulation, non small cell lung cancer

Introduction

Oncoprotein 18 (Op18)/stathmin is a highly conserved, cytoplasmic, small molecular phosphoprotein that is usually highly expressed in solid tumors (1). Op18 directly regulates the dynamic equilibrium of microtubule polymerization and depolymerization by inhibiting phosphorylation and activating dephosphorylation, which is closely associated with cell cycle, transport of substances, cell adhesion and migration, cell proliferation and differentiation, and cell death (2-4). Op18/stathmin has four phosphorylation sites, Ser16, Ser25, Ser38 and Ser63, which are regulated by a series of kinases, including cell division cycle-2 (CDC2; also termed cyclin-dependent kinase 1), extracellular-regulated protein kinase (ERK) of the mitogen-activated protein kinase family (5,6). Op18/stathmin integrates and relays multiple intra- and extracellular stimuli to mediate the maintenance of malignant phenotypes and other biological behaviors of tumor cells. Therefore, Op18 is a central target of a wide range of signaling pathways (7,8).

Our previous studies demonstrated that NCI-H1299 cells, a non-small cell lung cancer (NSCLC) cell line, with a high expression of Op18/stathmin has high resistance to Taxol (namely paclitaxel, which has been widely applied clinically as a cytoxic antiepithelioma chemotherapy drug derived from plants) compared with other epithelial-derived tumor cell lines (CNE1, MGC gastric cancer cells, MCF-7 breast cancer cells and Hep3b-2 hepatoma cells) (1). Additionally, silencing Op18/stathmin by RNA interference (RNAi) increased the sensitivity of NCI-H1299 cells to Taxol (1). Further *in vitro* experiments confirmed that autocrine interleukin-10 (IL-10) was decreased in NCI-H1299 cells when treated with a combination of Taxol and Op18/stathmin RNAi. In athymic *BALB/c* mice that lack functional mature T cells and have IL-10 production deficiency, autocrine IL-10 was identified to be produced by NCI-H1299 cell xenografts in the sera (9). Furthermore, Op18/stathmin RNAi and Taxol synergistically inhibited lung carcinogenesis and promoted the differentiation of implanted tumors and sensitivity to Taxol. The level of autocrine IL-10 was notably declined in the sera of tumor-bearing mice (9).

In this study, the possibility of autocrine IL-10 feedback regulating Op18/stathmin signaling in NCI-H1299 cells and its underlying molecular mechanisms were examined. The effects of cross talk between autocrine IL-10 and Op18/stathmin

signals on lung cancer malignant phenotypes, drug sensitivity and tumor immune escape were investigated.

Materials and methods

Cell culture. Human NSCLC NCI-H1299 cells (cat. no. CRL-5803; American Type Culture Collection, Manassas, VA, USA) were cultured in RPMI-1640 medium (cat. no. 01-100-1ACS; Biological Industries, Kibbutz Beit Haemek, Israel) supplemented with 10% fetal bovine serum (FBS; cat. no. 04-001-1ACS; Biological Industries), 100 IU/ml penicillin, and 100 μg/ml streptomycin (cat. no. sv30010; Hyclone; GE Healthcare Life Sciences, Logan, UT, USA) at 37˚C in a humidified atmosphere of 5% CO_2.

Antibodies and reagents. The primary antibodies used are as follows: Anti-Op18 (cat. no. 569391; Merck KGaA, Darmstadt, Germany); anti-phospho-Op18-Ser25 (cat. no. ab194752), anti-phospho-stathmin-Ser63 (cat. no. ab76583) and anti-IL-10 (cat. no. ab134742) from Abcam (Cambridge, MA, USA); anti-CDC2 p34 (cat. no. sc-954), anti-caspase-3 (cat. no. sc-7272), anti-ERK (cat. no. sc-93), anti-phospho-ERK (cat. no. sc-7383), anti-β-actin (cat. no. sc-47778) and anti-nuclear factor-κB (NF-κB; cat. no. sc-109) were from Santa Cruz Biotechnology, Inc. (Dallas, TX, USA); anti-phospho-Thr161-CDC2 (cat. no. 9114), anti-caspase-8 (cat. no. 9746), anti-caspase-9 (cat. no. 9502) and anti-phospho-Ser536-NF-κB p65 (cat. no. 3031S) were purchased from Cell Signaling Technology, Inc. (Danvers, MA, USA). The secondary antibodies were horseradish peroxidase (HRP)-conjugated goat anti-rabbit IgG (cat. no. sc-2004) and rabbit anti-mouse IgG (cat. no. sc-358914; Santa Cruz). NF-κB inhibitor pyrrolidine dithiocarbamate (PDTC; cat. no. 5108-96-3, Sigma-Aldrich; Merck KGaA) (10,11) and Taxol (cat. no. sc-201439; Santa Cruz Biotechnology, Inc.) were separately dissolved in dimethyl sulfoxide (DMSO) and stored at -20˚C.

Plasmid construction. RNAi targeting Op18/stathmin was used to silence Op18/stathmin. Small interfering RNA targeting the coding region of Op18/stathmin at 5'-AGAGAAACTGACCCACAAA-3' (GenBank no. 53305, sequence 374-393) were inserted into the *Bam*H1/*Hind*III restriction sites of pGCsilencer-U6/Neo/GFP (RNAi; Shanghai GeneChem Co., Ltd., Shanghai, China; sense gaAGAGAAACTGACCCACAAA, antisense TTTGTGGGTCAGTTTCTCTtc). A nonsense sequence not targeting any encoding gene was inserted into pGC-silencer-U6/Neo/GFP-Non (Non) and pGC-silencer-U6/Neo/GFP (Blank) was an empty plasmid. The plasmids (4 μg) were transiently transfected into cells at a transfection efficiency of >80% in 250 μl incomplete RPMI-1640 medium containing 10 μl Lipofectamine™ 2000 (Invitrogen; Thermo Fisher Scientific, Inc., Waltham, MA, USA); 4 h later, the medium replaced with complete medium for 24 h. All plasmids were previously constructed by our laboratory (9,12).

MTT assays. Cells were seeded in 96-well plates at 5,000 cells per well and supplemented with different concentrations of anti-IL-10 antibody (0, 0.5 and 2.5 μg/ml; cat. no. ab134742; Abcam). At 24, 48 and 72 h, 10 μl 0.5% MTT was added to the well and incubated at 37˚C for 4 h. The medium was then removed and 100 μl DMSO was added and incubated for 10 min. A total of six parallel wells/sample was used. The optical density (OD) value was measured using a microplate reader (BioTek Instruments, Inc., Winooski, VT, USA) at 490 nm. The relative proliferation ratios were calculated according to the formula: Relative proliferation ratio (%) = ($OD_{treatment}/OD_{control}$) x 100. Cells treated with DMSO were used as a control, and the OD value of the control was set as 1.0.

Colony formation assays. A total of 2,000 cells per well were seeded in a 6-well plate in the presence of anti-IL-10 antibody (0, 0.5 and 2.5 μg/ml) and incubated for 1-2 weeks. Cell growth was suspended when colonies were observed by the naked eye. The cells were fixed with 100% methanol for 10 min at room temperature and stained with 0.1% crystal violet at room temperature for 30 min. The colonies with >50 cells were counted with an inverted microscope. The relative colony formation efficiency was calculated using the formula: Relative colony formation efficiency (%) = (average colonies/2,000) x 100.

Wound healing assays. When the confluence of the cells was ~80%, the cells were washed three times with ice-cold phosphate-buffered saline (PBS). A sterilized pipette tip (200 μl) was applied to wipe off the cells along the longitudinal and parallel trails that were marked in the back of the plate. The plate was washed with PBS, and 0, 0.5 and 2.5 μg/ml anti-IL-10 antibody was added. Cell migration was observed with an inverted optical microscope at 0, 12, 24 and 36 h.

Transwell analysis. The upper Transwell chamber with 8.0 μm pore size of polycarbonate membrane of polystyrene plates (Costar; Corning Incorporated, NY, USA) was pretreated with heated serum-free RPMI-1640 for 30 min, and 800 μl complete medium containing 10% FBS was added to the lower chamber. A total of 10 μl cell suspension (cell density, $2x10^5$ cells/ml with 0.2% FBS of RPMI-1640) was added to the upper chamber at 37˚C for 24 h. The cells in the upper Transwell chamber were wiped with a cotton swab, and the cells were fixed with 100% methanol for 10 min and stained with 0.1% crystal violet for 10 min at room temperature. The cells that passed through the membrane were counted in five random visual fields under an inverted microscope. The migrated cells were then imaged and evaluated.

Flow cytometric analysis. A total of $2.5x10^5$ cells per well were seeded into 6-well plates in the presence of 2.5 μg/ml anti-IL-10 antibody combined with 100 nM Taxol. The cells were cultured for 24 h. The cells were harvested and fixed with 70% ethanol at 4˚C overnight for flow cytometric analysis. Cell apoptosis assay was performed using a Fluorescence Activating Cell Sorter (Beijing Dingguo Changsheng Biotechnology Co., Ltd., Beijing, China). In brief, cells were resuspended and stained in 500 μl binding buffer with 5 μl Annexin V-fluorescein isothiocyanate and 5 μl propidium following the instruction of Annexin V-fluorescein isothiocyanate Apoptosis Detection kit (Nanjing KeyGen Biotech Co.,

Ltd., Nanjing, China). In addition, the cells were treated with different concentrations (0, 5 and 10 μM) of PDTC for 24 h.

Western blot analysis. The cells were treated on ice with a cell lysis buffer (50 mM Tris-HCl, 1 mM ethylenediaminetetraacetic acid, 2% sodium dodecyl sulfate, 5 mM dithiothreitol and 10 mM phenylmethylsulfonyl fluoride) for 30 min. The lysates were collected and denatured in boiling water for 8 min and incubated on ice for 5 min. The lysates were sonicated for 30 sec and centrifuged at 4˚C for 15 min. The concentration of the protein was measured using BCA Protein Assay reagent (Pierce; Thermo Fisher Scientific Inc.). Total protein (50 μg) was separated by 10-12% SDS-polyacrylamide gel electrophoresis and electrotransferred onto a nitrocellulose membrane. The membrane was blocked for 2 h with 5% non-fat milk at room temperature in PBS with 0.05% Tween-20 and then incubated with primary antibodies, anti-β-actin (1:2,000), anti-Op18 (1:3,000), anti-phospho-Op18-Ser25, anti-phospho-stathmin-Ser63, anti-IL-10, anti-phospho-Thr161-CDC2, anti-CDC2 p34, anti-ERK, anti-phospho-ERK, anti-NF-κB, anti-phospho-Ser536-NF-κB p65, anti-caspase-3, anti-caspase-8 and anti-caspase-9 (all 1:1,000), overnight at 4˚C. The membrane was then incubated with HRP-conjugated secondary antibodies (1:2,000-1:3,000) for 1.5 h at room temperature. The membrane was visualized with an enhanced chemiluminescence detection kit (Thermo Fisher Scientific, Inc.).

ELISA assays. Cells in the logarithmic growth phase were seeded in 24-well plates. When the cells reached 80% confluence, the media was replaced with fresh RPMI-1640 medium. The cells were incubated in phenol red-free media for 6, 12, 24 and 36 h, while other cells were treated with 0, 5 and 10 μM PDTC in phenol red-free media for 24 h. The supernatant was collected for *in vitro* detection of autocrine IL-10. The human IL-10 ELISA kit [cat. no. EK1102; Multisciences (Lianke) Biotech Co., Ltd., Hangzhou, China] was used.

Animal experiments. Male Kunming mice (4-week-old) were randomly divided into four groups of 15, 30 and 45 day, and parallel controls (8 mice per group). NCI-H1299 cells at the logarithmic growth phase were collected and resuspended in normal saline. A total of $4x10^6$ cells in 0.5 ml were injected intraperitoneally into each mouse. The control mice were injected with the same volume of normal saline. Retro-orbital blood samples were collected from anaesthetized mice at day 0, 15, 30 and 45; the mice were respectively sacrificed at day 15, 30 and 45 at 15 days interval by cervical dislocation for the collection of blood. Flow cytometry (model no. BC-2800vet; Auto Hematology Analyzer; Shenzhen Mindray Bio-Medical Electronics Co., Ltd., Shenzhen, China) was performed to sort the leukocytes. Cell counting was performed by Servicebio, Inc. (Woburn, MA, USA).

In addition, part of each blood sample was used to detect IL-10 in the sera by ELISA. The mice were respectively sacrificed at day 15, 30 and 45 at 15 days interval by cervical dislocation for the collection of blood sample, and the tumors were removed from 45-day mice. The 3-5 μm thickness of tissue sections were fixed by 10% formalin overnight and stained with 10% hematoxylin (x5, 10 min) and 1% eosin (1 min) at room temperature and examined by inverted optical microscope. Histopathological examination was performed by Professor Deyun Feng (Department of Pathology, First Xiangya Hospital Affiliated to Central South University, Changsha, China).

Statistical analysis. Statistical analysis was performed using the SPSS 17.0 statistical software (SPSS, Inc., Chicago, IL, USA). The data are presented as the mean ± standard deviation. Analysis of variance and least significant difference method was applied to perform multiple comparisons between the groups, P<0.05 was considered to indicate a statistically significant difference.

Results

Anti-IL-10 antibody inhibits cell proliferation and colony formation. The relative proliferation ratios were 90.32, 85.54 and 82.02% at 24, 48 and 72 h in the presence of 0.5 μg/ml anti-IL-10 antibody, and 78.38, 73.38 and 66.60% at 2.5 μg/ml anti-IL-10 antibody. With the extension of time, the growth curve was steeper for 2.5 μg/ml compared with 0.5 μg/ml. The treatment with anti-IL-10 antibody inhibited cell proliferation in a dose-dependent manner (Fig. 1A). The histograms showed that the relative proliferation ratios of two treated groups were markedly lower compared with the control. In addition, the difference was also significant between two groups that were treated with anti-IL-10 antibody at three time points (P<0.01; Fig. 1B).

The colony formation analysis demonstrated that there were many large colonies with closely adhered cells in the control group. When the cells were exposed to the anti-IL-10 antibody, the number of colonies declined, and the cells became sparse. Only a few of small colonies appeared when treated with 2.5 μg/ml anti-IL-10 (Fig. 1C). The histograms indicated that the colony formation ratios were 11.95, 10.3 and 7.3% at 0, 0.5 and 2.5 μg/ml, respectively. There was no significant difference between the control and the group treated with 0.5 μg/ml anti-IL-10 (P>0.05). The number of colonies was significantly decreased in the group treated with 2.5 μg/ml anti-IL-10 antibody compared with the other two groups (P<0.01, Fig. 1D). The ELISA assays for autocrine IL-10 indicated that the OD values of the supernatants were 0.0845, 0.1115, 0.193 and 0.2285 at 6, 12, 24 and 36 h, respectively. The level of IL-10 reached a peak value at 36 h, which confirmed that the production of autocrine IL-10 was markedly increased with the increase in the duration of incubation in culture. The differences were statistically significant between 36 h and the other time points (Fig. 1E).

Cell migration is markedly inhibited in the presence of anti-IL-10. The wound healing experiments indicated that there were large blank areas at 12 h in all three groups. By 24 h, the blank areas became narrower, and the blank area was the narrowest in the 0 μg/ml control group. At 36 h, the wound nearly healed fully in the control group and was partially recovered at 0.5 μg/ml anti-IL-10 antibody; however, a large gap remained in the group treated with 2.5 μg/ml anti-IL-10 antibody (Fig. 2A). The Transwell analysis confirmed that the mean numbers of transmembrane cells per visual field were 21.4, 15.4 and 7.8 at 0, 0.5 and 2.5 μg/ml, respectively.

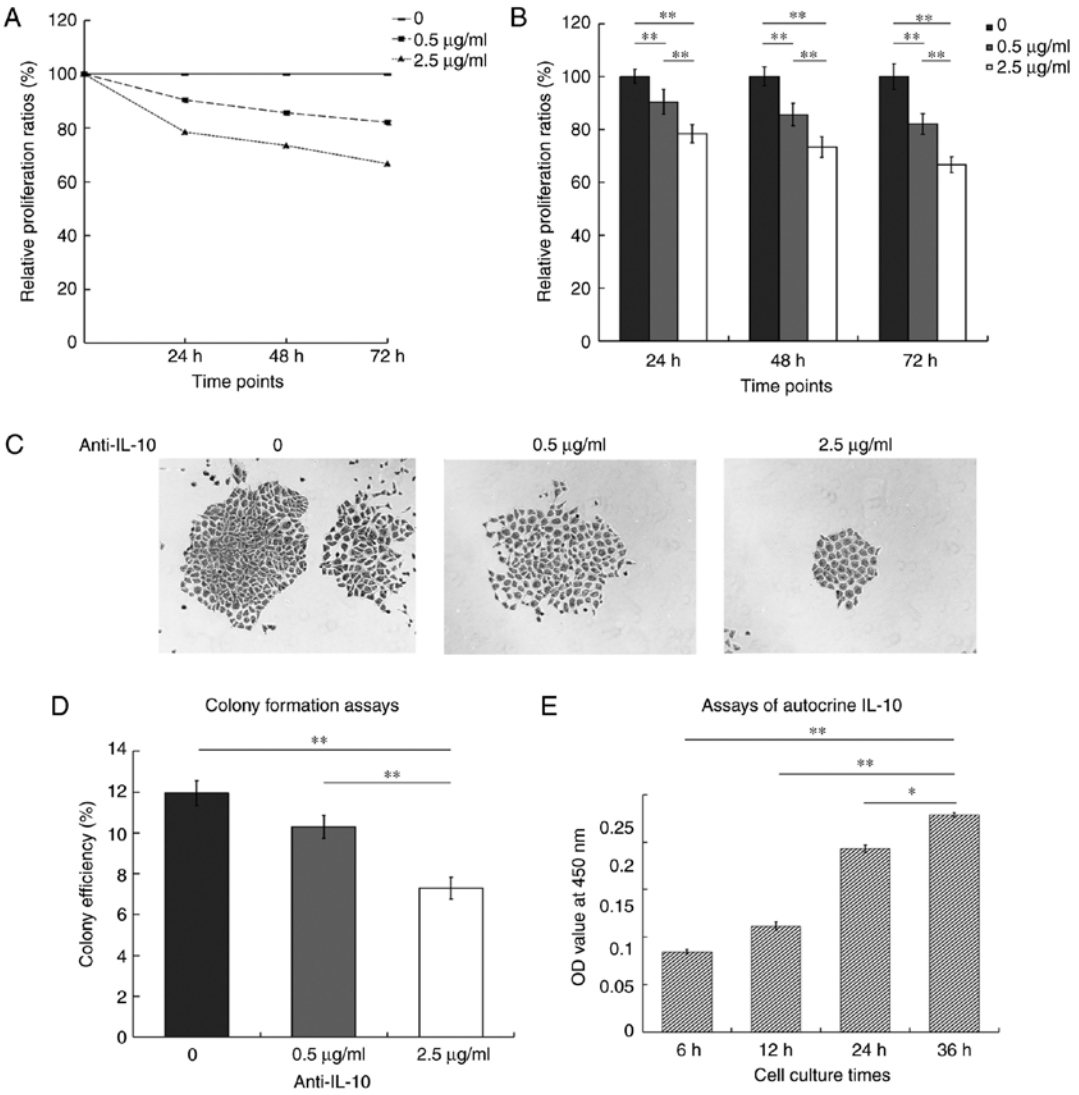

Figure 1. Anti-IL-10 antibody inhibits cell proliferation and colony formation. (A) Representative growth curves of NCI-H1299 cells treated with 0.5 and 2.5 μg/ml anti-IL-10. (B) Histograms showing the statistical differences of relative proliferation ratios at three time points. (C) Images of colony formation in NCI-H1299 cells treated with 0.5 and 2.5 μg/ml anti-IL-10 (original magnification, x100). (D) Histograms are indicating the differences in colony formation ratios among the three groups (E) ELISA assays for autocrine IL-10 release over time. Experiments were performed in triplicate. *P<0.05, **P<0.01. IL-10, interleukin-10; OD, optical density.

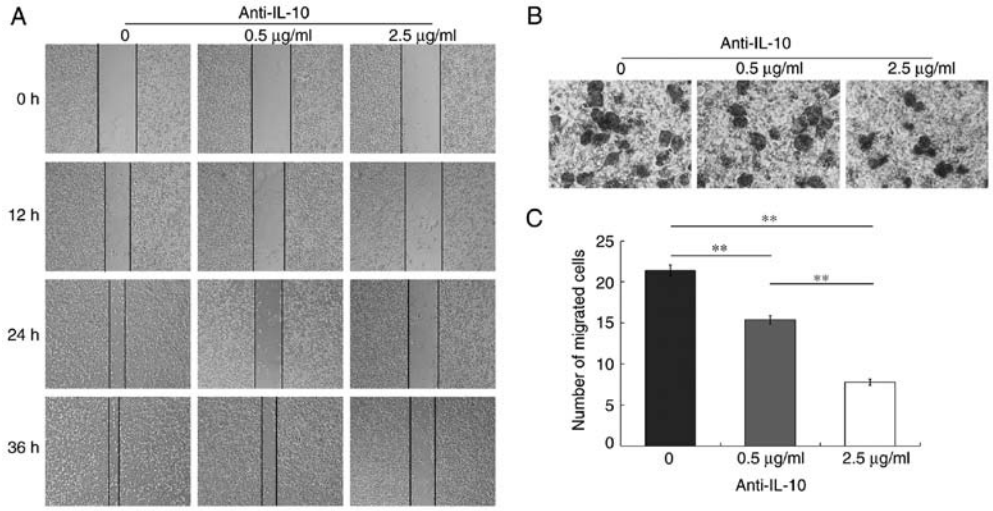

Figure 2. Neutralization of IL-10 arrests cell migration and invasion in 2-D and 3-D. (A) Status of migrated cells in 2-D planes (original magnification, x100). (B) Images of transmembrane cells in 3-D assay (original magnification, x400). (C) Histograms illustrated the statistical differences among the three groups treated with 0, 0.5 and 2.5 μg/ml of IL-10 antibody. Experiments were performed in triplicate. **P<0.01. IL-10, interleukin-10.

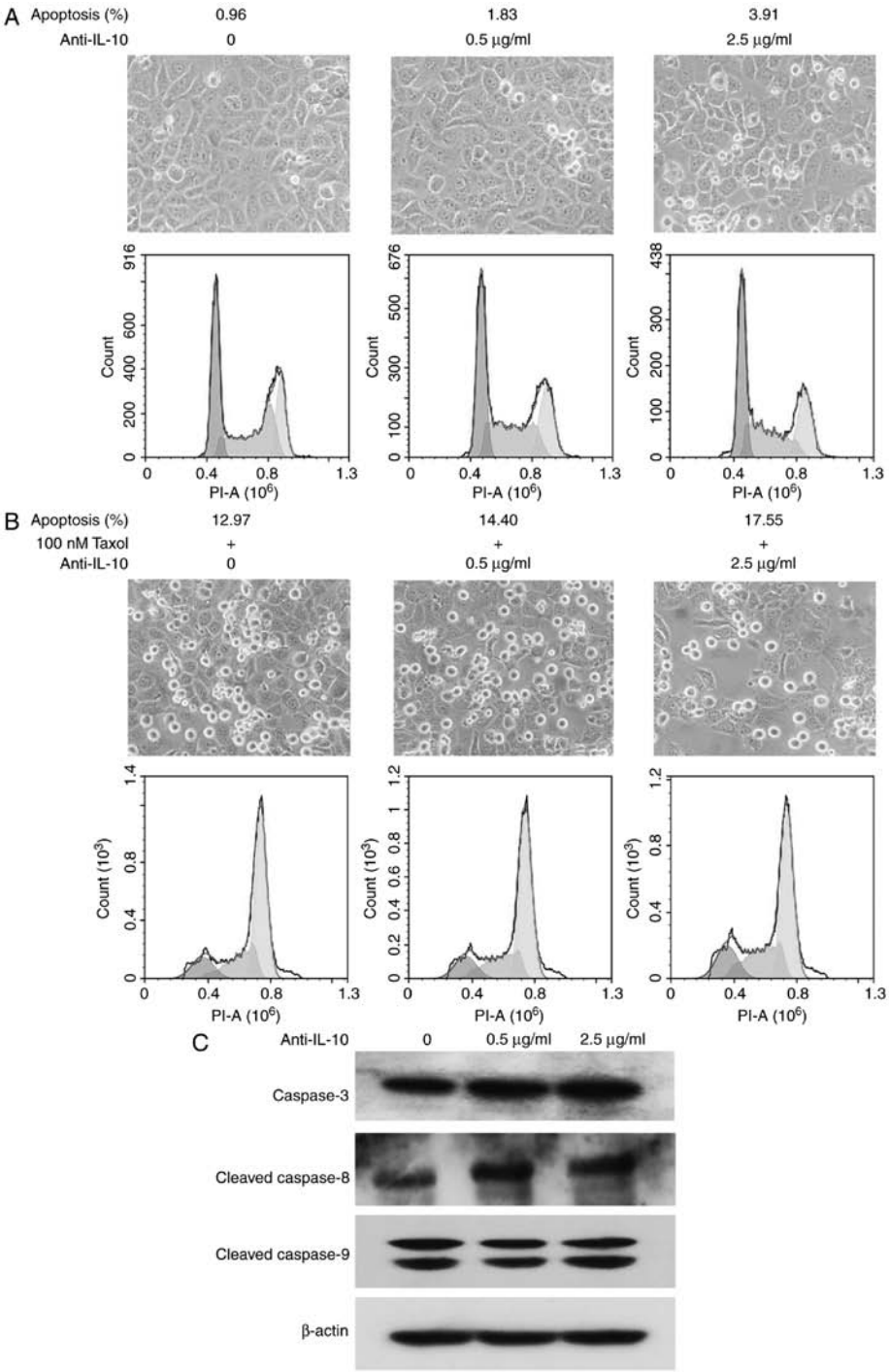

Figure 3. Anti-IL-10 antibody promotes cell apoptosis and the sensitivity to Taxol. (A) Upper panels present cell growth (original magnification, x200) and lower panels present cell apoptosis ratios from flow cytometric assays in cells treated with anti-IL-10. (B) Images of cell growth and apoptosis analysis by flow cytometry confirmed that anti-IL-10 antibody treatment enhanced the sensitivity of NCI-H1299 cells to Taxol in a dose-dependent manner (original magnification, x200 for images of cell growth). (C) Western blots of the expression of caspases-3, and cleaved caspase-8 and -9 in NCI-H1299 cells treated with anti-IL-10 antibody. IL-10, interleukin-10.

Invasion assay by Transwell demonstrated that the cells that invaded through the matrix on Transwell membranes were irregular in shape. The treatment with anti-IL-10 antibody led to the inhibition of cell migration in a 3-D format (Fig. 2B). The histograms indicated that the number of transmembrane cells was decreased in the two IL-10 antibody-treated groups compared with the control. The differences were significant in the group that was exposed to 2.5 μg/ml anti-IL-10 antibody compared with other two other groups ($P<0.01$; Fig. 2C).

Anti-IL-10 antibody promotes cell apoptosis and sensitivity to Taxol. Cell micrographs demonstrated that cells were arranged closely in the three groups, but a small number of floating cells appeared in the treated groups with the addition of anti-IL-10 antibody (indicating that anti-IL-10 antibody promoted cell apoptosis to some extent). Flow cytometric analysis demonstrated that cellular apoptotic rates were 0.96, 1.83 and 3.91% in the 0, 0.5 and 2.5 μg/ml treatment groups, respectively, which was slightly upregulated with the increase of anti-IL-10 antibody (Fig. 3A).

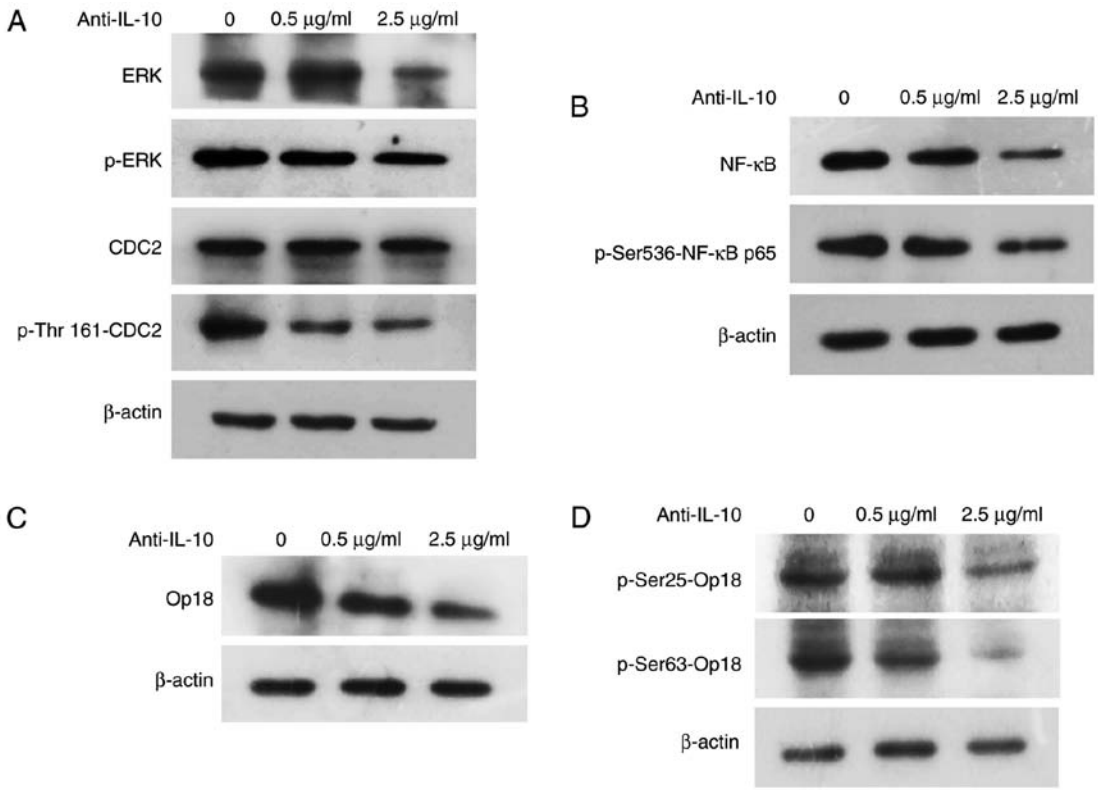

Figure 4. Neutralization of IL-10 downregulates Op18/stathmin expression and phosphorylation. (A) The expression and the phosphorylation of ERK and CDC2, (B) NF-κB and p-Ser563-NF-κB p65, (C) Op18/stathmin expression and (D) phosphorylation of Op18/stathmin at Ser25 and Ser63. IL-10, interleukin-10; ERK, extracellular signal-regulated kinase; p-, phospho-; CDC2, cell division cycle-2; NF-κB, nuclear factor-κB; Op18, oncoprotein 18.

A large number of cells became detached in the three groups treated with Taxol, cells became sparser with anti-IL-10 treatment, and the number of floating cells was highest in the group that received 2.5 μg/ml anti-IL-10 and Taxol. Flow cytometric assays demonstrated that cellular apoptotic ratios were 12.97, 14.40 and 17.55% at 0, 0.5 and 2.5 μg/ml anti-IL-10 antibody treatment, respectively, combined with 100 nM Taxol, which implied that neutralizing autocrine IL-10 promoted the sensitivity of NCI-H1299 cells to Taxol (Fig. 3B).

Western blot analysis demonstrated that anti-IL-10 induced the expression of caspase-3, and cleavage of caspase-8 in NCI-H1299 cells in a dose-dependent manner. However, there was no effect on caspase-9 expression or cleavage (Fig. 3C).

Neutralization of autocrine IL-10 decreases the activities of ERK, CDC2 and NF-κB, and reduces the expression and phosphorylation of Op18/stathmin. Western blot analysis demonstrated that the addition of anti-IL-10 decreased the expression and the phosphorylation of ERK, and the phosphorylation of CDC2 at Thr161. However, anti-IL-10 did not affect CDC2 expression, which indicated that the activities of ERK and CDC2, which are kinases upstream of Op18/stathmin, were weakened by neutralization of autocrine IL-10 *in vitro* (Fig. 4A). Similarly, anti-IL-10 antibody reduced the expression of NF-κB and its active subunit p65, which is phosphorylated at Ser536, in a dose-dependent manner (Fig. 4B). Further western blot detection identified that the expression of Op18/stathmin and its phosphorylated forms (Ser25 and Ser63) were gradually reduced with the increase of anti-IL-10 antibody concentration (Fig. 4C and D).

Blocking NF-κB signaling promotes cell apoptosis extent and decreases the activities of ERK and CDC2. To examine the relevance of the transcription factor, NF-κB and kinases (ERK and CDC2), PDTC, an inhibitor of NF-κB was applied to block NF-κB signaling. The cells grew sparsely in the presence of PDTC, with 10 μM PDTC as the highest concentration. Flow cytometric analysis showed that the apoptotic ratios were 1.34, 13.35 and 16.4% at 0, 5 and 10 μM PDTC, respectively (Fig. 5A).

Western blot analysis demonstrated that PDTC also decreased the expression and phosphorylation of ERK, and the phosphorylation of CDC2 at Thr161 in a concentration-dependent manner. However, PDTC did not exert any effects on CDC2 expression (Fig. 5B).

Blocking NF-κB or silencing Op18/stathmin reduces the levels of autocrine IL-10 and protein expression. ELISA assays for autocrine IL-10 demonstrated that the OD values of supernatants were 0.232, 0.21 and 0.168 at 0, 5 and 10 μM PDTC treatment, respectively. The levels of autocrine IL-10 were significantly downregulated at 10 μM PDTC compare with the 0 and 5 μM treatment groups ($P<0.01$; Fig. 6A). Western blot analysis indicated that PDTC also inhibited IL-10 protein expression in a concentration-dependent manner (Fig. 6B). Similarly, silencing Op18/stathmin by RNAi effectively reduced the expression of NF-κB and IL-10 (Fig. 6C).

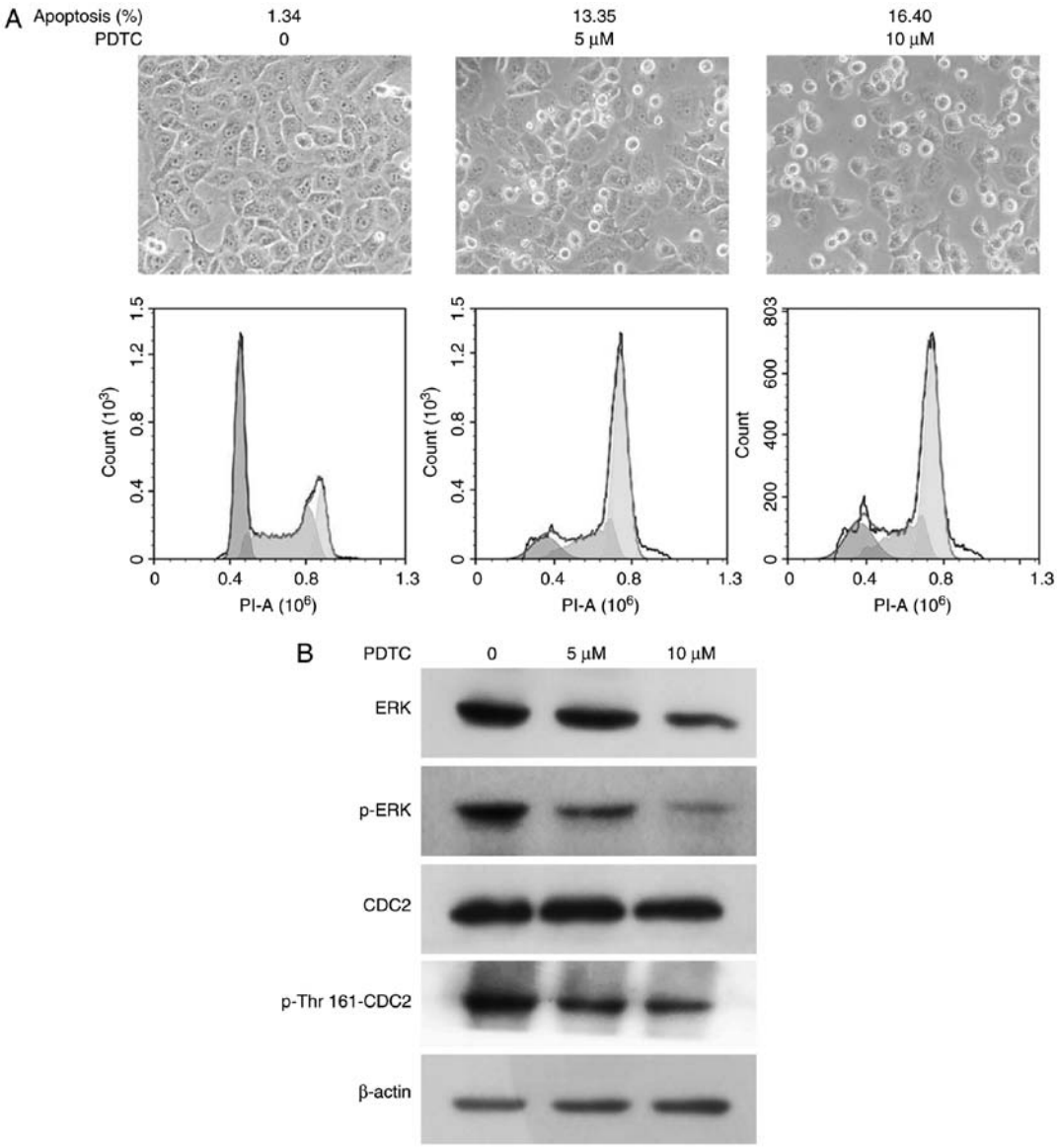

Figure 5. NF-κB inhibitor PDTC increases cell apoptosis and the decreases ERK and CDC2 activity. (A) Upper panels are showing cell growth (original magnification, x200). Lower panels are showing cell apoptosis ratios as detected by flow cytometric analysis. (B) Expression and phosphorylation of ERK and CDC2 as detected by western blotting. PDTC, pyrrolidine dithiocarbamate; ERK, extracellular signal-regulated kinase; p-, phospho-; CDC2, cell division cycle-2.

These findings suggested that blocking NF-κB or silencing Op18/stathmin inhibited the levels of IL-10 protein expression and autocrine release.

Release of autocrine IL-10 is involved in the reduction in neutrophils, lymphocytes and monocytes in the blood of xenografted mice. To examine whether autocrine IL-10 mediates tumor immune evasion, we collected the blood of mice with xenograft of NCI-H1299 cells on day 15, 30 and 45 for the detection of immune cells by flow cytometry. The average number of neutrophils was 2.800×10^9/l in the control mice. The number of neutrophils in mice that were inoculated was 2.300×10^9, 1.750×10^9 and 1.432×10^9 on day 15, 30 and 45, respectively. The number of neutrophils was significantly reduced on day 30 and 45 in tumor bearing mice compared with control mice ($P<0.01$; Fig. 7A). The number of lymphocytes in the four groups of mice was 5.575×10^9, 4.175×10^9, 3.925×10^9 and 2.425×10^9. The number of lymphocytes was significantly decreased on day 45 compared with the other time points and the control ($P<0.01$; Fig. 7B). The mean number of monocytes was 0.425×10^9, 0.325×10^9, 0.225×10^9 and 0.200×10^9 in the control, 15, 30 and 40 days groups. A significant difference in the number of monocytes was observed on day 30 and 45 compared with the control ($P<0.01$; Fig. 7C). Therefore, the number of neutrophils, lymphocytes and monocytes was all decreased in the blood of mice with xenografts. The levels of IL-10 were low in the sera on day 15 and similar to that of the control, which was gradually increased on day 30 and reached to the peak on day 45 (Fig. 7D).

The images of tumors indicated that the dissected tumors were identical in size in four random samples of mice with NCI-H1299 xenograft on day 45. Further histopathological examination identified that tumor tissues presented typical lung glandular cavity-like structure, and the cells were

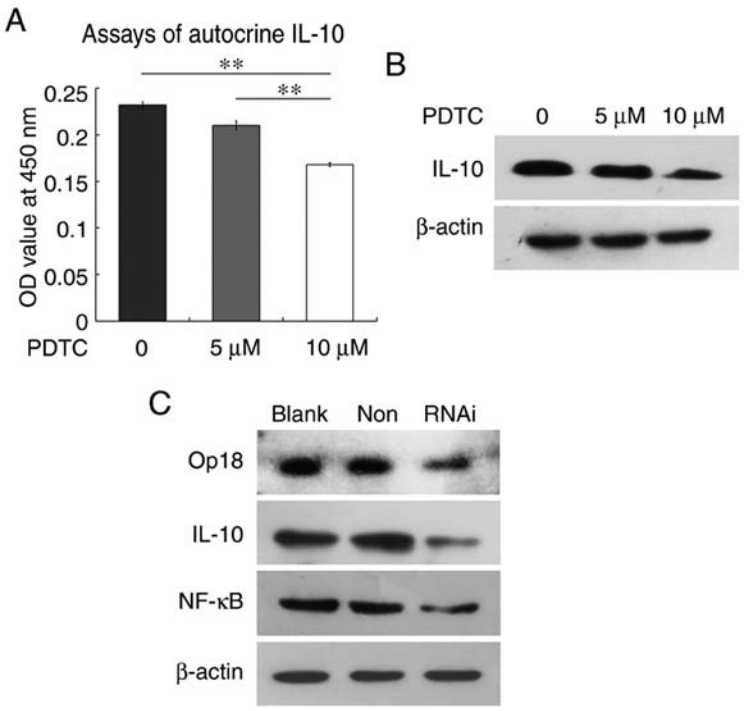

Figure 6. Inhibition of NF-κB or silencing Op18/stathmin signaling decreases the levels of IL-10 autocrine and protein expression. (A) Detection of autocrine IL-10 levels in cultured cells by ELISA. (B) Western blot analysis of IL-10 expression following treatment with PDTC. (C) Expression of IL-10 and NF-κB following RNAi silencing of Op18. **P<0.01. IL-10, interleukin-10; PDTC, pyrrolidine dithiocarbamate; OD, optical density; RNAi, RNA interference; Op18, oncoprotein 18; NF-κB, nuclear factor-κB.

heterogeneous in staining of the nuclei, which indicated that these tumors were derived from the lung adenocarcinoma epithelial NCI-H1299 cells that were intraperitoneally injected into the mice (Fig. 7E).

Discussion

It is well established that IL-10 is predominantly secreted by the T-helper 2 cell subpopulation, and it has a crucial role in humoral immune and inflammatory responses by stimulating the activation and proliferation of B lymphocytes and antibody production (13,14). Increasing evidence indicates that tumor cells may also secrete IL-10 that is involved in carcinogenesis and tumor immune evasion. Autocrine IL-10 predominantly functions to promote cell proliferation and metastasis, and tolerance to chemotherapeutics. IL-10 also exerts multiple immunosuppressive effects on host immune response (15,16).

In the present study, the levels of autocrine IL-10 were significantly increased with increased incubation duration of NCI-H1299 cells. *In vitro* neutralization of autocrine IL-10 resulted in the inhibition of cell proliferation, colony formation and cell migration. Anti-IL-10 also increased the expression of caspase-3 and cleavage of caspase-8, increased cell apoptosis and the sensitivity of NCI-H1299 cells to Taxol. This indicated that autocrine IL-10 is involved in tumor cell growth, cell metastasis and invasion as well as the development of resistance to Taxol. A previous study demonstrated that blocking autocrine IL-10 signaling led to the activation of exogenous cell death pathways via caspase-3 and -8 (17).

Other studies confirmed that the level of autocrine IL-10 secreted by tumor cells is involved associated with patient prognosis and curative effects of chemotherapeutics on patient prognosis. By contrast to with normal and benign tumor cells, the levels of IL-10 mRNA and protein expression are significantly higher in laryngeal cancer or melanoma cells (18,19). It was also previously demonstrated that overall survival was lowest in NSCLC patients with high serum levels of IL-10 in the compared with other cytokines (IL-1, IL-6, IL-8 and interferon-γ) (20). Patients with diffuse large B-cell lymphoma with elevated serum levels of IL-10 were likely to have tolerance to chemotherapy and poor clinical outcome. Inhibiting autocrine IL-10 using the non-toxic tellurium compound ammonium trichloro(dioxoethylene-O,O')tellurate enhanced the sensitivity of B and T-lymphoma cells to Taxol (21-23). Similarly, the level of autocrine IL-10 was positively associated with the malignancy of cervical cancer that is caused by human papillomavirus (24).

Our previous studies indicated that Op18/stathmin was a target of the kinases ERK and CDC2 in CNE1 cells. The Epstein-Barr virus-encoded the latent membrane protein 1 was demonstrated to regulate Op18/stathmin signaling by ERK and CDC2, which was associated with acceleration of cell cycle progression and cell proliferation. The levels of phospho-ERK and phospho-CDC2 Thr161 reflected the activities of ERK and CDC2 kinases (25,26). Blocking CDC2 signaling with Purvalanol A or ERK with PD98059 in NCI-H1299 cells decreased the phosphorylation of Op18/stathmin and the increase of sensitivity to Taxol in NCI-H1299 cells (27,28). This study identified that *in vitro* IL-10 neutralization negatively regulated the activities of ERK and CDC2 by reducing the phosphorylation of ERK and CDC2-Thr161, and decreased expression of Op18/stathmin and its phosphorylation at Ser25

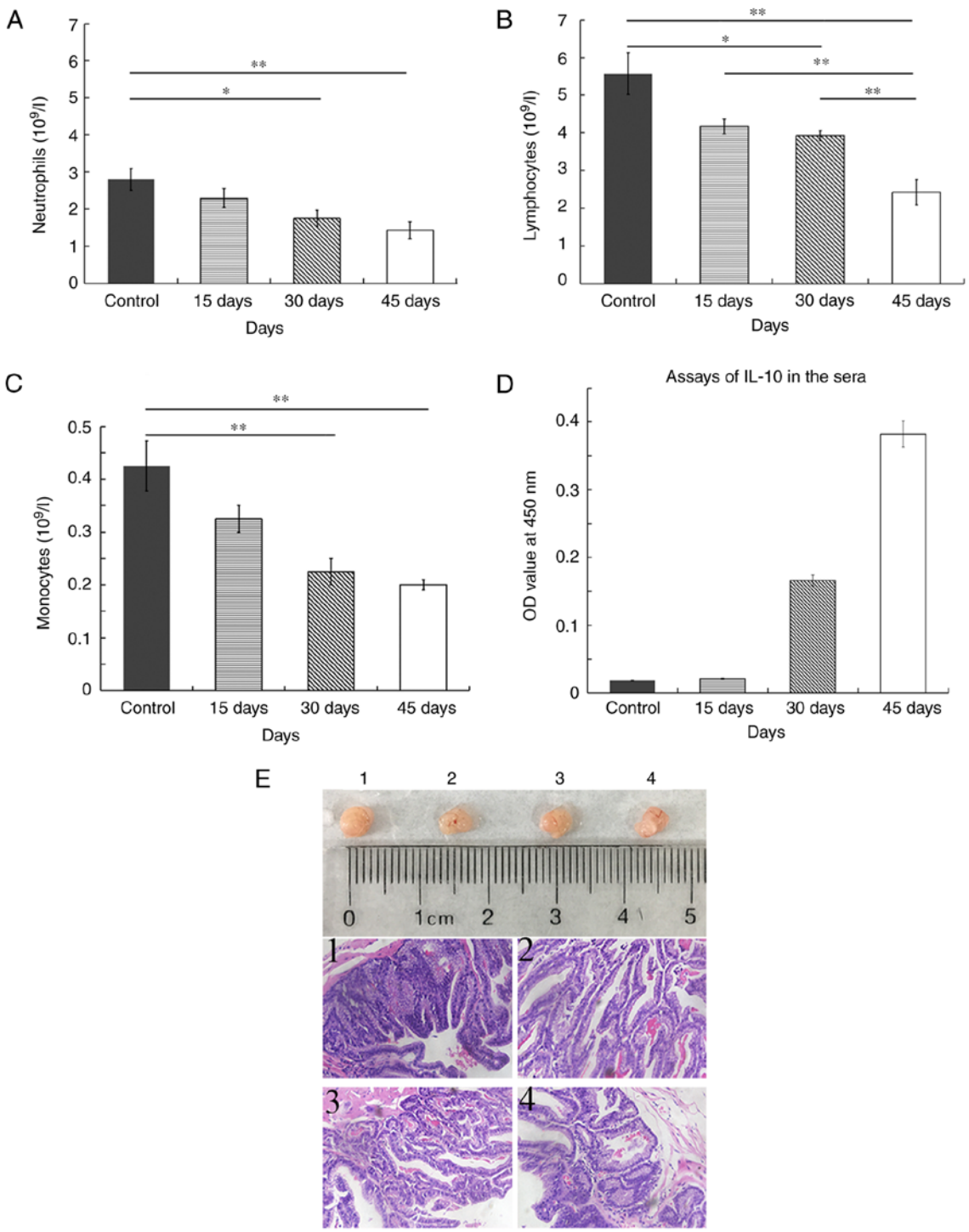

Figure 7. Detection of neutrophils, lymphocytes and monocytes in the blood of xenografted mice by fluorescence-activated cell sorting. Quantification of (A) neutrophils, (B) lymphocytes and (C) monocytes. (D) Analysis of IL-10 in the sera by ELISA. *P<0.05, **P<0.01. (E) Hematoxylin and eosin staining indicating the histopathological characteristics of dissected tumors from the mice with xenografts on day 45 (original magnification, x400). IL-10, interleukin-10; OD, optical density.

and Ser63, however anti-IL-10 also induced downregulation of ERK expression. Whether the reduced ERK phosphorylation was caused by decreased total expression requires further investigation. In short, anti-IL-10 also increased the sensitivity of NCI-H1299 cells to Taxol via regulation of ERK and CDC2 signaling.

Transcription factor NF-κB is closely associated with cell proliferation, of which NF-κB p65 is the main active subunit. The phosphorylation of p65 Ser536 is well established as a marker of NF-κB activation, which has an important role in tumorigenesis (29,30). In SW-1990 pancreatic cancer cells, silencing Op18/stathmin downregulated NF-κB p65 and NF-κB expression, and induced the arrest of cell proliferation and metastasis (31). In cervical cancer, serine protease inhibitor, kallikrein, markedly impeded NF-κB activation by suppressing NF-κB inhibitor α degradation and the phosphorylation of p65,

which led to the inhibition of cell growth (32). Our previous studies indicated that silencing Op18/stathmin by targeting RNAi-inhibited IL-10 autocrine in CNE1 and NCI-H1299 cells enhanced the sensitivity of the cells to Taxol (9,12). This study demonstrated that *in vitro* neutralizing autocrine IL-10 attenuated NF-κB expression and activity. Blocking NF-κB signaling using the inhibitor, PDTC, led to a decrease in the activities of ERK and CDC2, and a decrease in the levels of autocrine IL-10 and protein expression. Op18/stathmin RNAi also decreased the expression of NF-κB and IL-10 in NCI-H1299 cells, which suggested the presence of an autocrine IL-10/NF-κB/ERK/CDC2/Op18/stathmin axis and a positive feedback loop between Op18/stathmin and autocrine IL-10. The regulation of Op18/stathmin signaling mediated by autocrine IL-10 may be important for the maintenance of malignant tumor behaviors in NCI-H1299 cells.

Autocrine IL-10 is usually regarded as an immune inhibitory cytokine, which induces tumor immune evasion by reducing the activation of antigen-presenting cells (33). In MC38 cell mouse colon cancer models, the killing effects of cytotoxic T cells were markedly reduced when the serum level of autocrine IL-10 was increased (34). In chronic gastric mucosal infections caused by *Helicobacter pylori*, the maturation of dendritic cells (DCs) and antigen delivery was inhibited by inducing the autocrine secretion of IL-10 from DCs, ultimately leading to evasion of the host immune surveillance by *Helicobacter pylori* and the development of gastric cancer (35). In breast tumors, the high level of IL-10 secreted by tumor-associated macrophages was demonstrated to significantly prevent paclitaxel-induced apoptosis of breast tumor cells. Neutralizing IL-10 using anti-IL-10 antibody resulted in the attenuation of signal transducer and activator of transcription 3 activation and decreased Bcl-2 mRNA expression. This consequently enhanced the sensitivity of breast cancer cells (36). The animal experiments in the current study indicated that the number of neutrophils, lymphocytes and monocytes were significantly decreased in the blood of mice with NCI-H1299 cell xenografts at 45 days after inoculation. The release of IL-10 was increased with the occurrence and growth of xenografted tumors. This finding suggested that autocrine IL-10 reduced the generation of neutrophils, lymphocytes and monocytes, and thus affected neutrophil-mediated inflammation, antigen processing, presentation of monocytes and the immune effects of B- or T-lymphocytes, which ultimately resulted in tumor immune evasion. The associated molecular mechanism required further investigation.

Acknowledgements

We thank Professor Feng Deyun from the First Affiliated Xiangya Hospital of Central South University (Changsha, China) for histopathological examination.

Funding

This study was financed by the Key Scientific Research Project of Colleges and Universities of Hunan Province (grant no. 12A018), the National Natural Science Foundation of China (grant no. 81272274) and the Natural Science Foundation of Hunan Province (grant no 12JJ3104).

Availability of data and materials

The datasets used and/or analyzed during the current study are available from the corresponding author on reasonable request.

Authors' contributions

XL was mainly responsible for the design of the study and revision of the manuscript. The experiments, analysis and interpretation of the data were mainly carried out by YZ. SC, FS, DL, TY, MW, as members of the research team, participated in part of the experiments, analysis and interpretation of the data. All authors read and approved the final manuscript.

Ethics approval and consent to participate

All animal experiments were reviewed and approved by the Ethics Committee of Center for Scientific Research with Animal Models of Changsha Medical University, Hunan, China (no. 2017-05-1). All applicable international, national and institutional guidelines for the care and use of animals were followed.

Patient consent for publication

Not applicable.

Competing interests

The authors declare that they have no competing interests.

References

1. Lin X, Liao Y, Xie J, Liu S, Su L and Zou H: Op18/stathmin is involved in the resistance of taxol among different epithelial carcinoma cell lines. Cancer Biother Radiopharm 29: 376-386, 2014.
2. Yip YY, Yeap YY, Bogoyevitch MA and Ng DC: Differences in c-Jun N-terminal kinase recognition and phosphorylation of closely related stathmin-family members. Biochem Biophys Res Commun 446: 248-254, 2014.
3. Machado-Neto JA, Lazarini M, Favaro P, de Melo Campos P, Scopim-Ribeiro R, Franchi Junior GC, Nowill AE, Lima PR, Costa FF, Benichou S, *et al*: ANKHD1 silencing inhibits Stathmin 1 activity, cell proliferation and migration of leukemia cells. Biochim Biophys Acta 1853: 583-593, 2015.
4. Machado-Neto JA, de Melo Campos P, Favaro P, Favaro P, Lazarini M, Lorand-Metze I, Costa FF, Olalla Saad ST and Traina F: Stathmin 1 is involved in the highly proliferative phenotype of high-risk myelodysplastic syndromes and acute leukemia cells. Leuk Res 38: 251-257, 2014.
5. Nemunaitis J: Stathmin 1: A protein with many tasks. New biomarker and potential target in cancer. Expert Opin Ther Targets 16: 631-634, 2012.
6. Johnsen JI, Aurelio ON, Kwaja Z, Jörgensen GE, Pellegata NS, Plattner R, Stanbridge EJ and Cajot JF: p53-mediated negative regulation of stathmin/Op18 expression is associated with G_2/M cell-cycle arrest. Int J Cancer 88: 685-691, 2000.
7. Ke B, Wu LL, Liu N, Zhang RP, Wang CL and Liang H: Overexpression of stathmin 1 is associated with poor prognosis of patients with gastric cancer. Tumour Biol 34: 3137-3145, 2013.
8. Watanabe A, Suzuki H, Yokobori T, Tsukagoshi M, Altan B, Kubo N, Suzuki S, Araki K, Wada S, Kashiwabara K, *et al*: Stathmin 1 regulates p27 expression, proliferation and drug resistance, resulting in poor clinical prognosis in cholangiocarcinoma. Cancer Sci 105: 690-696, 2014.

9. Long D, Yu T, Chen X, Liao Y and Lin X: RNAi targeting STMN alleviates the resistance to taxol and collectively contributes to down regulate the malignancy of NSCLC cells in vitro and in vivo. Cell Biol Toxicol 34: 7-21, 2017.
10. Lee EH, Kim SS and Seo SR: Pyrrolidine dithiocarbamate (PDTC) inhibits inflammatory signaling via expression of regulator of calcineurin activity 1 (RCAN1): Anti-inflammatory mechanism of PDTC through RCAN1 induction. Biochem Pharmacol 143: 107-117, 2017.
11. Ko EY, Cho SH, Kwon SH, Eom CY, Jeong MS, Lee W, Kim SY, Heo SJ, Ahn G, Lee KP, *et al*: The roles of NF-kappaB and ROS in regulation of pro-inflammatory mediators of inflammation induction in LPS-stimulated zebrafish embryos. Fish Shellfish Immunol 68: 525-529, 2017.
12. Lin X, Yu T, Zhang L, Chen S, Chen X, Liao Y, Long D and Shen F: Silencing Op18/stathmin by RNA interference promotes the sensitivity of nasopharyngeal carcinoma cells to taxol and high-grade differentiation of xenografted tumours in nude mice. Basic Clin Pharmacol Toxicol 119: 611-620, 2016.
13. Cheng SB and Sharma S: Interleukin-10: A pleiotropic regulator in pregnancy. Am J Reprod immunol 73: 487-500, 2015.
14. Heine G, Drozdenko G, Grun JR, Chang HD, Radbruch A and Worm M: Autocrine IL-10 promotes human B-cell differentiation into IgM- or IgG-secreting plasmablasts. Eur J Immunol 44: 1615-1621, 2014.
15. Ledeboer A, Breve JJ, Wierinckx A, van der Jagt S, Bristow AF, Leysen JE, Tilders FJ and Van Dam AM: Expression and regulation of interleukin-10 and interleukin-10 receptor in rat astroglial and microglial cells. Eur J Neurosci 16: 1175-1185, 2002.
16. Rodriguez JA, Galeano L, Palacios DM, Gómez C, Serrano ML, Bravo MM and Combita AL: Altered HLA class I and HLA-G expression is associated with IL-10 expression in patients with cervical cancer. Pathobiology 79: 72-83, 2012.
17. Sakamaki K, Imai K, Tomii K and Miller DJ: Evolutionary analyses of caspase-8 and its paralogs: Deep origins of the apoptotic signaling pathways. Bioessays 37: 767-776, 2015.
18. Itakura E, Huang RR, Wen DR, Paul E, Wunsch PH and Cochran AJ: IL-10 expression by primary tumor cells correlates with melanoma progression from radial to vertical growth phase and development of metastatic competence. Mod Pathol 24: 801-809, 2011.
19. Mahipal A, Terai M, Berd D, Chervoneva I, Patel K, Mastrangelo MJ and Sato T: Tumor-derived interleukin-10 as a prognostic factor in stage III patients undergoing adjuvant treatment with an autologous melanoma cell vaccine. Cancer Immunol Immunother 60: 1039-1045, 2011.
20. Barrera L, Montesservín E, Barrera A, Ramírez-Tirado LA, Salinas-Parra F, Bañales-Méndez JL, Sandoval-Ríos M and Arrieta Ó: Cytokine profile determined by data-mining analysis set into clusters of non-small-cell lung cancer patients according to prognosis. Ann Oncol 26: 428-435, 2015.
21. Gupta M, Han JJ, Stenson M, Maurer M, Wellik L, Hu G, Ziesmer S, Dogan A and Witzig TE: Elevated serum IL-10 levels in diffuse large B-cell lymphoma: A mechanism of aberrant JAK2 activation. Blood 119: 2844-2853, 2012.
22. Lech-Maranda E, Baseggio L, Bienvenu J, Charlot C, Berger F, Rigal D, Warzocha K, Coiffier B and Salles G: Interleukin-10 gene promoter polymorphisms influence the clinical outcome of diffuse large B-cell lymphoma. Blood 103: 3529-3534, 2004.
23. Danoch H, Kalechman Y, Albeck M, Longo DL and Sredni B: Sensitizing B- and T-cell lymphoma cells to paclitaxel/abraxane-induced death by AS101 via inhibition of the VLA-4-IL10-survivin axis. Mol Cancer Res 13: 411-422, 2015.
24. Bermudez-Morales VH, Peralta-Zaragoza O, Alcocer-Gonzalez JM, Moreno J and Madrid-Marina V: IL-10 expression is regulated by HPV E2 protein in cervical cancer cells. Mol Med Rep 4: 369-375, 2011.
25. Lin X, Tang M, Tao Y, Li L, Liu S, Guo L, Li Z, Ma X, Xu J and Cao Y: Epstein-Barr virus-encoded LMP1 triggers regulation of the ERK-mediated Op18/stathmin signaling pathway in association with cell cycle. Cancer Sci 103: 993-999, 2012.
26. Lin X, Liu S, Luo X, Ma X, Guo L, Li L, Li Z, Tao Y and Cao Y: EBV-encoded LMP1 regulates Op18/stathmin signaling pathway by cdc2 mediation in nasopharyngeal carcinoma cells. Int J Cancer 124: 1020-1027, 2009.
27. Lin X, Liao Y, Chen X, Long D, Yu T and Shen F: Regulation of oncoprotein 18/stathmin signaling by ERK concerns the resistance to taxol in nonsmall cell lung cancer cells. Cancer Biother Radiopharm 31: 37-43, 2016.
28. Chen X, Liao Y, Long D, Yu T, Shen F and Lin X: The Cdc2/Cdk1 inhibitor, purvalanol A, enhances the cytotoxic effects of taxol through Op18/stathmin in non-small cell lung cancer cells in vitro. Int J Mol Med 40: 235-242, 2017.
29. Hoesel B and Schmid JA: The complexity of NF-kappaB signaling in inflammation and cancer. Mol Cancer 12: 86, 2013.
30. Chen JY, He XX, Ma C, Wu XM, Wan XL, Xing ZK, Pei QQ, Dong XP, Liu DX, Xiong WC, *et al*: Netrin-1 promotes glioma growth by activating NF-kappaB via UNC5A. Sci Rep 7: 5454, 2017.
31. Lu Y, Liu C, Cheng H, Xu Y, Jiang J, Xu J, Long J and Liu L, Yu X: Stathmin, interacting with Nf-kappaB, promotes tumor growth and predicts poor prognosis of pancreatic cancer. Curr Mol Med 14: 328-339, 2014.
32. Wang T, Shi F, Wang J, Liu Z and Su J: Kallistatin Suppresses cell proliferation and invasion and promotes apoptosis in cervical cancer through blocking NF-kappaB signaling. Oncol Res 25: 809-817, 2017.
33. Mittal SK and Roche PA: Suppression of antigen presentation by IL-10. Curr Opin Immunol 34: 22-27, 2015.
34. Tanikawa T, Wilke CM, Kryczek I, Chen GY, Kao J, Núñez G and Zou W: Interleukin-10 ablation promotes tumor development, growth, and metastasis. Cancer Res 72: 420-429, 2012.
35. Rizzuti D, Ang M, Sokollik C, Wu T, Abdullah M, Greenfield L, Fattouh R, Reardon C, Tang M, Diao J, *et al*: *Helicobacter pylori* inhibits dendritic cell maturation via interleukin-10-mediated activation of the signal transducer and activator of transcription 3 pathway. J Innate Immun 7: 199-211, 2015.
36. Yang C, He L, He P, Liu Y, Wang W, He Y, Du Y and Gao F: Increased drug resistance in breast cancer by tumor-associated macrophages through IL-10/STAT3/bcl-2 signaling pathway. Med Oncol 32: 352, 2015.